Supporting Information

Heterogeneous reaction kinetics influencing benzo(a)pyrene global atmospheric distribution and related lifetime lung cancer risk

Mega Octaviani[1,2,§,*], Benjamin A. Musa Bandowe[1], Qing Mu[1,3], Jake Wilson[1], Holger Tost[4], Hang Su[1], Yafang Cheng[1], Manabu Shiraiwa[5], Ulrich Pöschl[1], Thomas Berkemeier[1,*], Gerhard Lammel[1,6,*]

[1]Max Planck Institute for Chemistry, Multiphase Chemistry Department, Mainz, Germany
[2]Karlsruhe Institute of Technology, Institute of Meteorology and Climate Research, Department Troposphere Research, Karlsruhe, Germany
[3]Xi'an Jiaotong-Liverpool University, Department of Health and Environmental Sciences, Suzhou, China
[4]University of Mainz, Institute of Atmospheric Physics, Mainz, Germany
[5]University of California, Department of Chemistry, California, USA
[6]Masaryk University, Research Centre for Toxic Compounds in the Environment, Brno, Czech Republic

[§]Now at Swedish Meteorological and Hydrological Institute, Norrköping, Sweden

*Correspondence to mega.octaviani@smhi.se, t.berkemeier@mpic.de, g.lammel@mpic.de

S1. Parameterization of BaP multiphase degradation rate

Table S1. Parameterization of multiphase degradation of BaP with ozone in the ROI-T scheme.[1] First-order reaction rate coefficients $k(\ s^{-1})$ given as $k = \text{base} + \frac{\text{max-base}}{1+\left(\frac{x\text{half}}{[O_3]}\right)^{\text{rate}}}$ with $[O_3]$ in ppbv. For each grid cell, the parameters are read from the look-up table with temperature (T) and relative humidity (RH) closest to the T and RH of the grid cell. When equally close, the smaller parameter value is adopted. Adapted from Table S3 in Mu et al.[1]

70%RH				
***T* (°C)**	**base**	**max-base**	**rate**	**xhalf**
40	1.67×10^{-4}	1.29×10^{-2}	0.682	1.25×10^{3}
35	1.19×10^{-4}	1.29×10^{-2}	0.682	1.25×10^{3}
30	8.52×10^{-5}	9.02×10^{-3}	0.696	1.23×10^{3}
25	5.94×10^{-5}	6.33×10^{-3}	0.707	1.27×10^{3}
23	4.84×10^{-5}	5.14×10^{-3}	0.700	1.25×10^{3}
15	2.55×10^{-5}	2.72×10^{-3}	0.711	1.29×10^{3}
10	1.58×10^{-5}	1.68×10^{-3}	0.706	1.27×10^{3}
5	9.49×10^{-6}	1.00×10^{-3}	0.698	1.24×10^{3}
0	6.85×10^{-6}	5.64×10^{-4}	0.704	1.11×10^{3}
-5	5.31×10^{-6}	3.10×10^{-4}	0.713	1.01×10^{3}
-10	3.83×10^{-6}	1.48×10^{-4}	0.731	7.33×10^{2}
-15	8.93×10^{-7}	1.05×10^{-4}	0.580	1.88×10^{3}
-20	1.16×10^{-6}	2.58×10^{-5}	0.673	3.35×10^{2}
50%RH				
***T* (°C)**	**base**	**max-base**	**rate**	**xhalf**
40	1.65×10^{-4}	1.80×10^{-2}	0.672	1.21×10^{3}
35	1.16×10^{-4}	1.27×10^{-2}	0.678	1.24×10^{3}
30	8.24×10^{-5}	8.68×10^{-3}	0.688	1.22×10^{3}
25	5.44×10^{-5}	5.71×10^{-3}	0.688	1.21×10^{3}
23	2.64×10^{-5}	3.08×10^{-3}	0.618	7.97×10^{2}
15	2.20×10^{-6}	1.10×10^{-3}	0.544	5.83×10^{2}
10	7.84×10^{-7}	2.60×10^{-4}	0.559	7.50×10^{1}

5	-4.79×10^{-7}	7.19×10^{-5}	0.564	1.31×10^{1}
0	-7.02×10^{-6}	2.18×10^{-5}	0.464	1.05
-5	-4.06×10^{-6}	6.54×10^{-6}	0.459	1.24×10^{-1}
-10	-1.89×10^{-6}	2.02×10^{-6}	0.429	1.44×10^{-2}
-15	2.58×10^{-7}	7.22×10^{-7}	0.175	1.28×10^{-1}
-20	1.79×10^{-7}	2.60×10^{-7}	0.689	1.11×10^{3}
Dry				
$T(^{\circ}\mathrm{C})$	**base**	**max-base**	**rate**	**xhalf**
40	1.61×10^{-4}	1.74×10^{-2}	0.667	1.19×10^{3}
35	1.10×10^{-4}	1.19×10^{-2}	0.667	1.21×10^{3}
30	6.75×10^{-5}	7.31×10^{-3}	0.653	1.11×10^{3}
25	2.3×10^{-5}	3.10×10^{-3}	0.586	7.02×10^{2}
23	-1.90×10^{-5}	9.28×10^{-4}	0.446	1.59×10^{2}
15	-2.65×10^{-5}	3.09×10^{-4}	0.341	8.38×10^{1}
10	-4.28×10^{-5}	1.03×10^{-4}	0.191	4.41
5	-1.12×10^{-5}	3.49×10^{-5}	0.142	4.33
0	3.39×10^{-6}	1.03×10^{-5}	0.382	8.85×10^{2}
-5	1.37×10^{-6}	5.67×10^{-6}	0.780	2.96×10^{3}
-10	4.53×10^{-7}	1.57×10^{-6}	0.979	1.63×10^{3}
-15	1.44×10^{-7}	2.10×10^{-6}	0.924	1.39×10^{4}

Table S2. First-order multiphase degradation rate of the ozonolysis of uncoated BaP for laboratory-derived schemes of: Pöschl et al. 2001[2], Kwamena et al. 2004[3], Kahan et al. 2006[4]. The reaction rate coefficient $k = \frac{k_{\max} k_{O_3}[O_3]}{1+k_{O_3}[O_3]}$ is in s^{-1}. For Kahan et al. 2006 scheme, $k = \frac{A \times [O_3]}{B+[O_3]}$ in s^{-1}. $[O_3]$ is in molec cm^{-3}. Adapted from Table S1 in Mu et al.[1]

Scheme	**Substrate**	$\mathbf{O_3}$ **(ppmv)**	$\boldsymbol{T}$ **(K)**	**RH** (%)	$\boldsymbol{k_{max}}$ $\mathbf{(s^{-1})}$	$\boldsymbol{k_{O_3}}$ $\mathbf{(1 \times 10^{-15} cm^3)}$
Pöschl et al. 2001	spark discharge soot	$0.05 - 1$	296 ± 2	0	0.015 ± 0.001	270 ± 40
				25	0.016 ± 0.001	280 ± 20
Kwamena et al. 2004	azelaic acid	$2 - 45$	298 ± 5	0	0.048 ± 0.008	1.2 ± 0.4
				72	0.060 ± 0.018	2.8 ± 1.4
	NaCl	$2 - 45$	298 ± 5	0	0.032	< 0.12
Kahan et al. 2006	octanol	$15 - 950$	room	0	$A = (5.5 \pm 0.2) \times 10^{-3}$ s^{-1}	$B = (2.8 \pm 0.4) \times 10^{15}$ molec cm^{-3}

S2. Spatial distribution of BaP atmospheric column burden

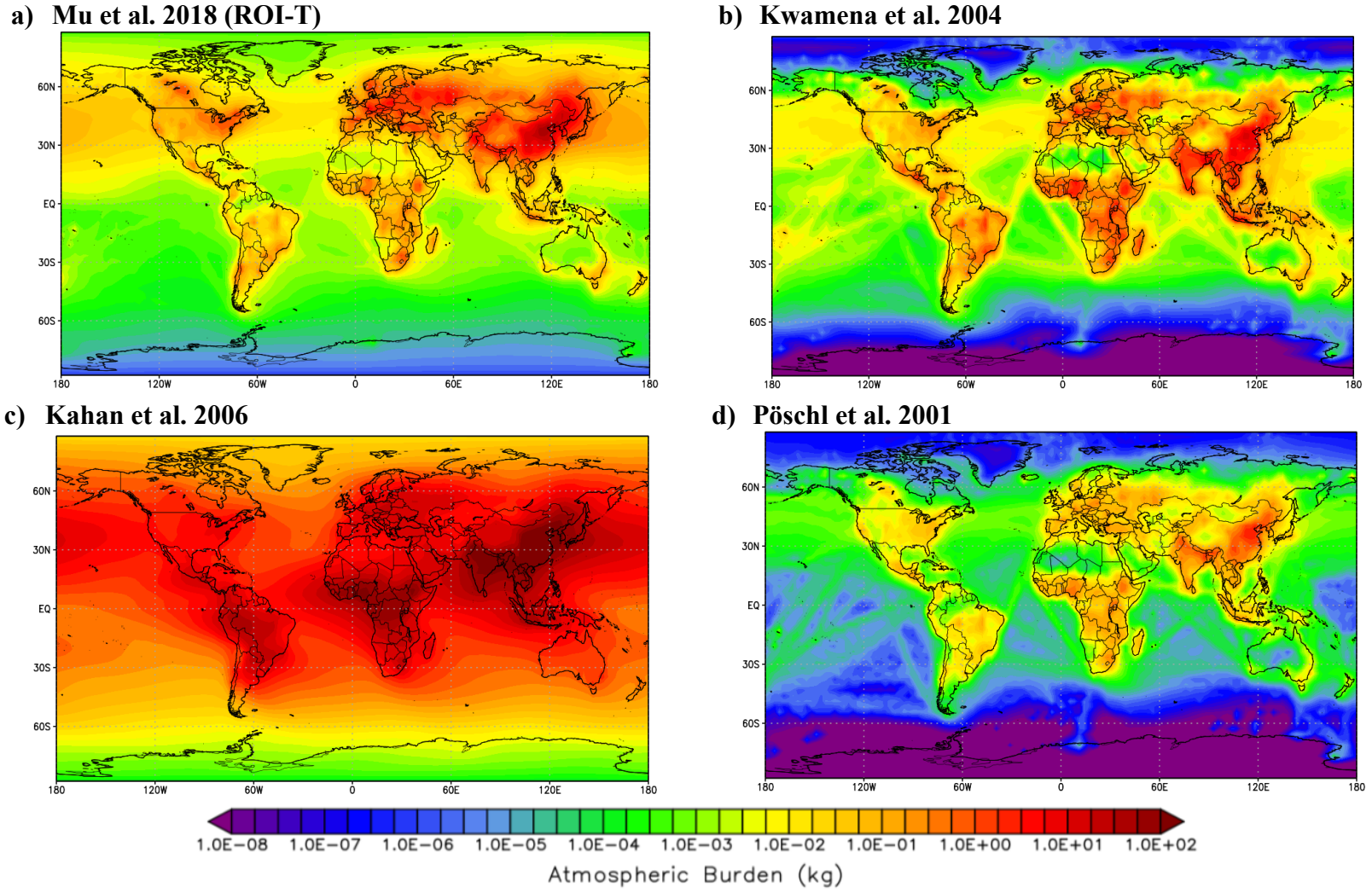

Figure S1. Atmospheric column burden of BaP (kg) over ~2.8×2.8° horizontal grid cells averaged over the years 2007-2009.

S3. Model evaluation

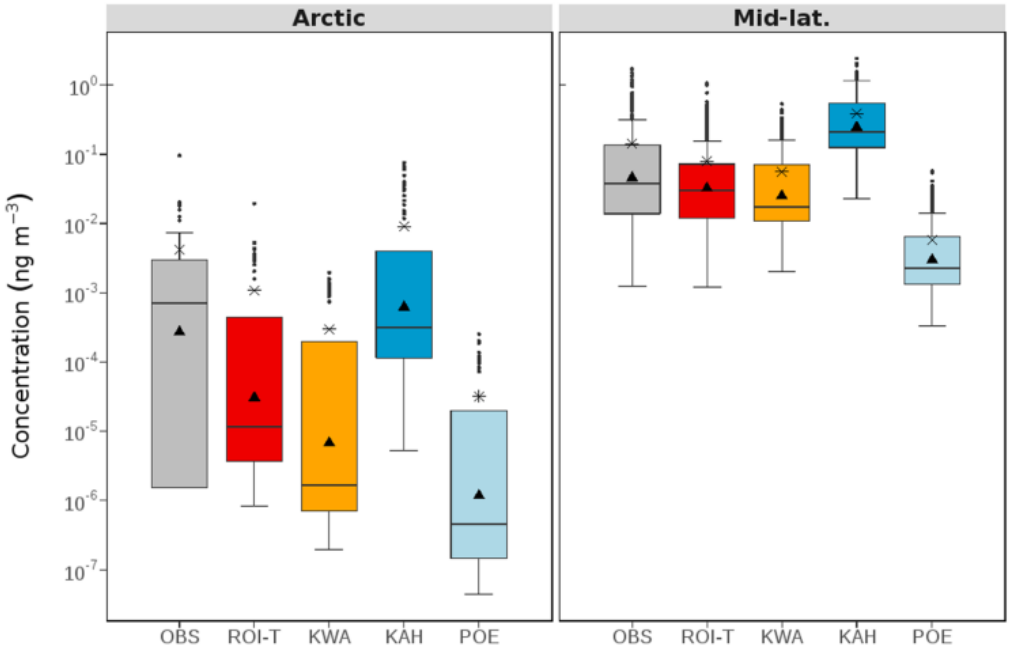

Figure S2. Box-and-whisker plots representing the distributions of BaP concentrations (ng m^{-3}) from observations (OBS) and simulations by the Mu et al. 2018 (ROI-T), Kwamena et al. 2004 (KWA), Kahan et al. 2006 (KAH), and Pöschl et al. 2001 (POE) schemes. Monthly data from all stations in the (left) Arctic and (right) mid-latitudes over the years 2007-2009. The boxes represent the interquartile range (IQR; difference between the 1st and 3rd quartiles), the middle lines are the median, the whiskers are the highest and lowest values that are not outliers, dots are the outliers (values outside 1.5×IQR above the 3rd quartile and below the 1st quartile), asterisks are the arithmetic means, and triangles are the geometric means.

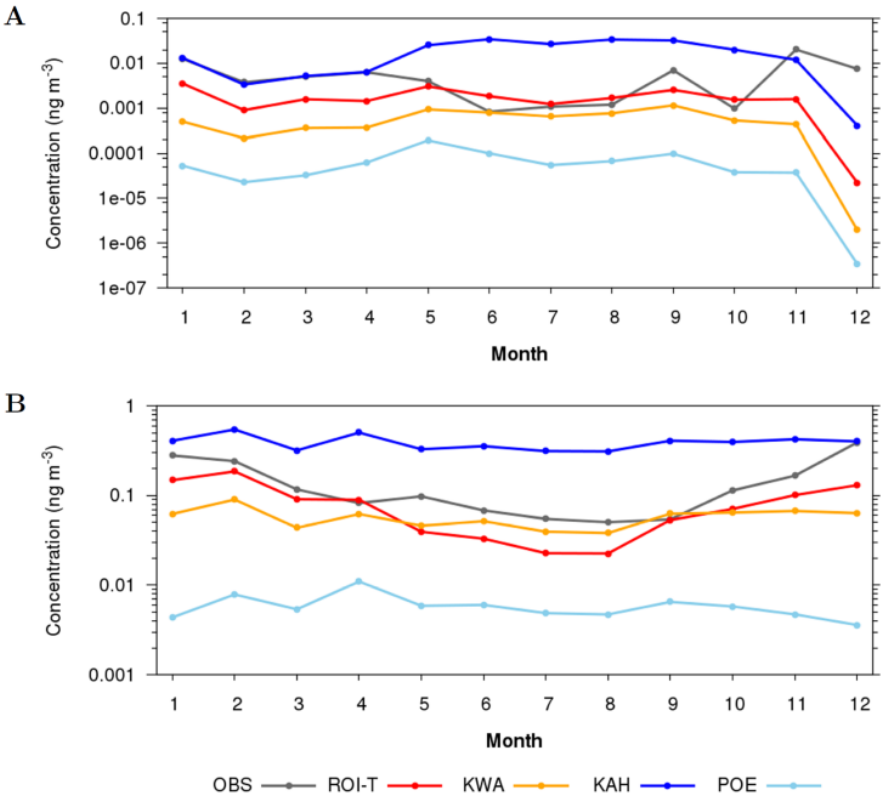

Figure S3. Seasonal mean BaP concentrations (ng m^{-3}) from observations and simulations by the Mu et al. 2018 (ROI-T), Kwamena et al. 2004 (KWA), Kahan et al. 2006 (KAH), and Pöschl et al. 2001 (POE) schemes, averaged over all stations in the (A) Arctic and (B) mid-latitudes for the year 2007-2009.

S4. Vertical distribution of regional-mean BaP

Figure S4 reveals significant regional variations in the distribution of BaP concentrations as influenced by different heterogeneous schemes. The Arctic and Antarctic regions stand out with distinct characteristics, both compared to the global average and to other regions (Figures S4a,e). In these polar regions, the Kwamena et al. 2004 and Pöschl et al. 2001 schemes demonstrate a pronounced decline in BaP concentrations with increasing altitude, particularly from above the boundary layer up to the free troposphere, whereas the Mu et al. 2018 (ROI-T) and Kahan et al. 2006 schemes show only marginal changes in BaP concentrations. In contrast to the Arctic and Antarctic, other regions such as the Northern and Southern mid-latitudes (Figures S4b,c) and the tropics (Figure S4d) exhibit BaP concentration trends with height that are more in line with the global average. The sharp decline in BaP concentrations in polar regions by the two schemes can be attributed to two factors. Firstly, the high atmospheric stability in these regions restricts vertical mixing and results in strong stratification, causing BaP to remain concentrated near the surface. Secondly, the efficient oxidation of BaP in the Kwamena et al. 2004 and Pöschl et al. 2001 schemes plays a role in its decline at higher altitudes. However due to lower solar radiation levels, the reduced regional O_3 concentration limits the oxidation of BaP, resulting in its persistence within boundary layer. Overall, these factors account for the distinct pattern of BaP vertical concentrations in polar regions compared to other regions.

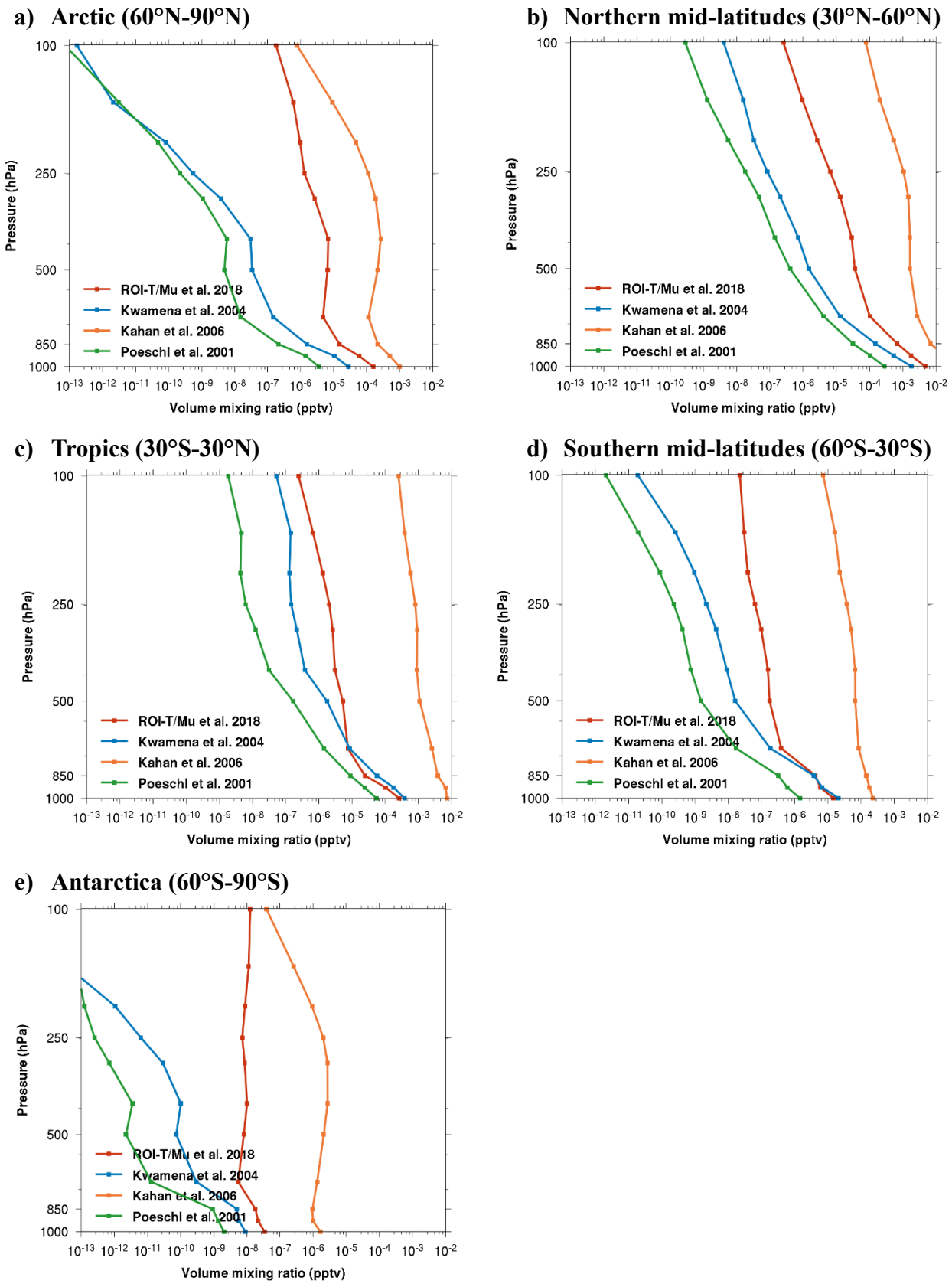

Figure S4. Vertical profiles of regional mean BaP volume mixing ratio (pptv) averaged over the period 2007-2009.

S5. Compartmental distribution

The predicted distribution of BaP in ocean and terrestrial surface compartments is shown in Table S5. Under the ROI-T scheme, the global surface burden is ~249 Mg, with soils accounting for the majority at 53% (133 Mg), while 28%, 15%, and 2.5% are stored in ocean, vegetation, and snow and glacier, respectively. Under the Kwamena et al. 2004 and Kahan et al. 2006 schemes, less is predicted in soils (35% and 25%, respectively) and more in the ocean (42% and 56%, respectively).

Considering the global atmospheric burden of BaP at ~1.6 Mg (Table S3), the total environmental burden, which includes both atmospheric and surface compartments, amounts to ~250 Mg under the ROI-T. This corresponds to ~6% of the annual emissions in 2008 (4509 Mg). The total environmental burden calculated with the Pöschl et al. 2001 scheme is the smallest (59 Mg), followed by the Kwamena et al. 2004 scheme (151 Mg), whereas the Kahan et al. 2006 scheme yields a much higher value (7461 Mg). Accordingly, the environmental residence times, calculated as the burden divided by the annual emissions, are 20, 5 and 12 days under the ROI-T, Pöschl et al. 2001 and Kwamena et al. 2004 schemes, respectively, but 20 months under the Kahan et al. 2006 scheme.

In an earlier modeling study, using a different (but similar) global multicompartment model, global atmospheric lifetime and total environmental burden were estimated higher with 81 days and 22% of annual (1996) emissions, respectively. The compartmental distribution in that study attributed 46% of the total environmental burden to vegetation, 44% to soils, 7.8% to ocean, and 2.5% to air.[5]

According to the ROI-T scheme, a substantial share of the total environmental burden, around 6%, is found in the Arctic while the Antarctic is least affected with only 0.006% (the area shares of polar regions are ~4% of the globe's area). The BaP compartmental distribution in the Arctic is primarily in soil (52%), followed by the ocean (23%), vegetation (17%), and ice sheets (7.5%). Note that sea-ice was neglected in the model, which creates a modest overestimation (<5%) of the oceanic share in compartmental distributions of low volatile and lipophilic substances[6]. The total deposition flux to the Arctic is 0.68 ng m^{-2} d^{-1}, which corresponds to 14.8% of the global net deposition flux, or almost four times the area share. As BaP degradation in surface compartments will be slower in the Arctic than globally – biodegradation rates are

roughly halving per -10 K – this high share of BaP depositions indicates long-term accumulation in the Arctic environment, unexpected for lipophilic substances partitioning mostly to the particulate phase[7].

Table S3. Global and regional atmospheric BaP burdens, (a) absolute (kg), and (b) relative to the global burden (%)

a.

Region	Burden within 1000-10 hPa				Burden within 1000-850 hPa			
	ROI-T/ Mu et al. 2018	**Kwamena et al. 2004**	**Kahan et al. 2006**	**Pöschl et al. 2001**	**ROI-T/ Mu et al. 2018**	**Kwamena et al. 2004**	**Kahan et al. 2006**	**Pöschl et al. 2001**
Arctic (60°N-90°N)	29.1	3.27	497	0.44	11.9	1.43	149	0.21
Northern mid-latitudes (30°N-60°N)	1,321	296	20,805	67	598	92	7350	27
Tropics (30°S-30°N)	218	472	42,036	59	48	140	14,639	18
Southern mid-latitudes (60°S-30°S)	8.03	8.49	618.35	0.68	3.53	3.72	247.11	0.29
Antarctic (90°S-60°S)	0.03	<0.01	3.50	<0.01	<0.01	<0.01	0.28	<0.01
Global	1,577	779	63,959	128	662	237	22,386	45

b.

Region	Burden within 1000-10 hPa				Burden within 1000-850 hPa			
	ROI-T/ Mu et al. 2018	**Kwamena et al. 2004**	**Kahan et al. 2006**	**Pöschl et al. 2001**	**ROI-T/ Mu et al. 2018**	**Kwamena et al. 2004**	**Kahan et al. 2006**	**Pöschl et al. 2001**
Arctic (60°N-90°N)	1.84	0.42	0.78	0.35	1.79	0.60	0.67	0.47
Northern mid-latitudes (30°N-60°N)	83.8	37.9	32.5	52.7	90.4	38.7	32.8	60.0
Tropics (30°S-30°N)	13.8	60.6	65.7	46.5	7.28	59.1	65.4	38.9
Southern mid-latitudes (60°S-30°S)	0.51	1.09	0.97	0.53	0.53	1.57	1.10	0.63
Antarctic (90°S-60°S)	<0.01	<0.01	0.01	<0.01	<0.01	<0.01	<0.01	<0.01

Table S4. Global and regional atmospheric lifetime (hours) due to chemistry. Annual and seasonal means.

	Mu et al. 2018 (ROI-T)	Kwamena et al. 2004	Kahan et al. 2006	Pöschl et al. 2001
Global				
Annual	4.97	2.14	155.50	0.08
DJF	11.05	2.21	153.08	0.09
JJA	1.33	2.20	162.31	0.08
Arctic (60°N-90°N)				
Annual	12.24	2.10	164.24	0.10
DJF	26.66	2.22	186.87	0.10
JJA	2.52	2.33	154.35	0.10
Northern mid-latitudes (30°N-60°N)				
Annual	6.49	2.01	151.00	0.08
DJF	15.31	2.32	171.33	0.10
JJA	1.16	1.91	142.69	0.07
Tropics (30°S-30°N)				
Annual	1.78	2.21	159.36	0.08
DJF	2.90	2.06	140.88	0.08
JJA	1.39	2.36	180.30	0.09
Southern mid-latitudes (60°S-30°S)				
Annual	2.23	2.27	177.87	0.10
DJF	1.50	2.34	187.22	0.11
JJA	3.40	2.22	172.62	0.10
Antarctic (90°S-60°S)				
Annual	43.48	2.44	224.16	0.12
DJF	26.52	2.89	227.82	0.16
JJA	48.30	2.16	224.40	0.10

Table S5. Global and regional ocean and terrestrial surface burdens (kg) averaged over 2007-2009. n.a. = not applicable.

	ROI-T/ Mu et al. 2018	Kwamena et al. 2004	Kahan et al. 2006	Pöschl et al. 2001
Ocean				
1. Global	70,610	63,604	4,178,180	15,837
2. Arctic	3,405	560	48,874	126
3. Antarctic	13.1	3.81	1,751	0.95
Soil				
1. Global	133,486	52,134	1,861,390	26,405
2. Arctic	7,710	1,549	78,610	542
3. Antarctic	n.a.	n.a.	n.a.	n.a.
Vegetation				
1. Global	38,780	34,542	1,393,490	16,096
2. Arctic	2,574	599	34,904	178
3. Antarctic	n.a.	n.a.	n.a.	n.a.
Snow and glacier				
1. Global	6,295	1,144	27,854	468
2. Arctic	1,112	153	8,828	59.2
3. Antarctic	1.94	0.55	217	0.24

S6. Cancer risk characterization

Figure S5 shows LLCR estimates for all four kinetic schemes and shows roughly a two order of magnitude spread between the low and high estimates. For example, in central Europe, LLCR varies from 1 to 100 additional cancer cases per one million population over an assumed lifetime of approximately 70 years, corresponding to a LLCR range of 1×10^{-6} to 1×10^{-4}. In central and eastern China, the LLCR ranges from approximately 1×10^{-5} to 1×10^{-3}. In this study, the risk value of one in a million (1×10^{-6}) is generally considered an *insignificant* risk and is used as a maximum permissible environmental risk. On the other hand, a risk value exceeding 100 in a million (1×10^{-4}) is considered *high* risk. Risk values falling between these two levels are characterized as posing a *potential* risk. Levels in the EU exceed the value of 1×10^{-4} are considered within an acceptable range of additional lifetime risk level.[8]

Consistent with the findings related to environmental and atmospheric column burden, the Pöschl et al. 2001 scheme yields the smallest LLCR estimates, while the Kahan et al. 2006 scheme generates the highest. The differences in LLCR estimates between these two schemes span a range of one to three orders of magnitudes. Specifically, in the Kahan et al. 2006 scheme, high-risk regions include central and eastern China, India, the Indochina Peninsula, parts of southwestern Russia and Central Africa. The LLCR estimates from the Kwamena et al. 2004 and ROI-T schemes fall within the range observed in the Pöschl et al. 2001 and Kahan et al. 2006 schemes. Notably, the Kwamena et al. 2004 scheme tends to produce higher risk levels in regions within the latitude range of 30°S-30°N compared to the ROI-T scheme, suggesting that most parts of Brazil and Central Africa are areas with potential risk of elevated LLCR.

These findings highlight the substantial variability in LLCR estimates resulting from different kinetic schemes, thereby underscoring the importance of the role of heterogeneous oxidation and inherent uncertainties involved. This understanding is crucial when evaluating the potential health risks associated with BaP and other comparable pollutants.

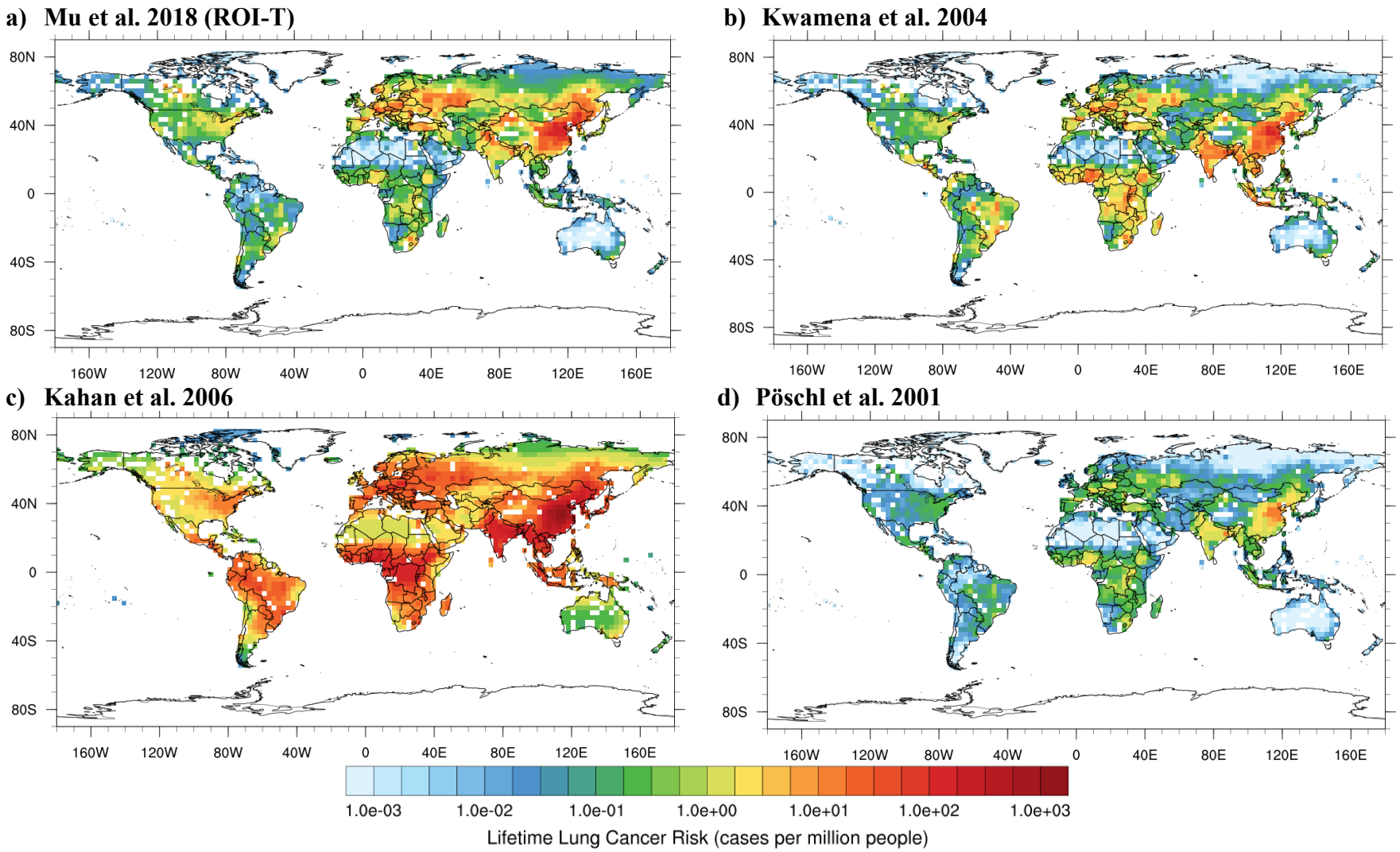

Figure S5. Estimated lifetime lung cancer risks (LLCR) for BaP expressed as additional cancer cases per million people exposed

References

1. Mu, Q.; Shiraiwa, M.; Octaviani, M.; Ma, N.; Ding, A.; Su, H.; Lammel, G.; Pöschl, U.; Cheng, Y., Temperature effect on phase state and reactivity controls atmospheric multiphase chemistry and transport of PAHs. *Sci. Adv.* **2018,** *4* (3).

2. Pöschl, U.; Letzel, T.; Schauer, C.; Niessner, R., Interaction of ozone and water vapor with spark discharge soot aerosol particles coated with benzo[a]pyrene: O3 and H2O adsorption, benzo[a]pyrene degradation, and atmospheric Implications. *J. Phys. Chem. A* **2001,** *105* (16), 4029-4041.

3. Kwamena, N.-O. A.; Thornton, J. A.; Abbatt, J. P. D., Kinetics of surface-bound benzo[a]pyrene and ozone on solid organic and salt aerosols. *J. Phys. Chem. A* **2004,** *108* (52), 11626-11634.

4. Kahan, T. F.; Kwamena, N. O. A.; Donaldson, D. J., Heterogeneous ozonation kinetics of polycyclic aromatic hydrocarbons on organic films. *Atmos. Environ.* **2006,** *40* (19), 3448-3459.

5. Lammel, G.; Sehili, A. M.; Bond, T. C.; Feichter, J.; Grassl, H., Gas/particle partitioning and global distribution of polycyclic aromatic hydrocarbons – A modelling approach. *Chemosphere* **2009,** *76* (1), 98-106.

6. Guglielmo, F.; Stemmler, I.; Lammel, G., The impact of organochlorines cycling in the cryosphere on their global distribution and fate – 1. Sea ice. *Environ. Pollut.* **2012,** *162*, 475-481.

7. Wania, F., Potential of degradable organic chemicals for absolute and relative enrichment in the Arctic. *Environ. Sci. Technol.* **2006,** *40* (2), 569-577.

8. European Union. Working Group on Polycyclic Aromatic Hydrocarbons *Ambient air pollution by Polycyclic Aromatic Hydrocarbons (PAH). Position Paper*; Office for official publications of the European Communities: Luxembourg, 2001; p 56.